

An Automated Approach to Detect Oceanic Eddies From Satellite Remotely Sensed Sea Surface Temperature Data

Changming Dong, Francesco Nencioli, Yu Liu, and James C. McWilliams

Abstract—Cyclonic (anticyclonic) oceanic eddies drive local upwelling (downwelling), leaving footprints in the sea surface temperature (SST) field as local extremes. Satellite-measured SST images can therefore be used to obtain information of the characteristics of oceanic eddies. Remotely sensed measurements represent very large data sets, both spatially and temporally. Manual eddy detection and analysis are thus practically impossible. In this letter, an automated scheme for eddy detection from remote sensing SST data is presented. The method is based on the analysis of velocity fields derived from SST measurements (thermal-wind velocity field). Using the geometric features of the velocity field, we can identify positions of eddy centers and derive eddy size, intensity, path, and lifetime. The scheme is applied to a realistic remotely sensed SST data set in a strong eddy activity region: Kuroshio Extension region.

Index Terms—Eddy, remote sensing, sea surface temperature (SST).

I. INTRODUCTION

CYCLONIC (anticyclonic) eddies drive local upwelling (downwelling), leaving a footprint on the sea surface temperature (SST) field as cold (warm) core features. Satellite-measured SST images carrying these anomalies can therefore be used to obtain information on the characteristics of oceanic eddies. This could help us to better understand the processes involved in eddy generation, evolution and decaying, and their impacts on marine environment and climate change. Given

Manuscript received February 22, 2011; revised April 7, 2011; accepted April 25, 2011. Date of publication June 20, 2011; date of current version October 28, 2011. The work of C. Dong was supported in part by the National Science Foundation (OCE 06-23011) and in part by the National Aeronautics and Space Administration under Grant NNX08AI84G. The work of Y. Liu was supported in part by the Knowledge Innovation Program of the Chinese Academy of Sciences (KZCX1-YW-12-4), in part by the National Basic Research Program of China (2007CB411801), and in part by the National Science Foundation (OCE 06-23011). The work of F. Nencioli was supported in part by the National Aeronautics and Space Administration under Grant NNX08AI84G.

C. Dong and J. C. McWilliams are with the Institute of Geophysics and Planetary Physics, University of California, Los Angeles, CA 90095 USA (e-mail: cdong@atmos.ucla.edu; jcm@atmos.ucla.edu).

F. Nencioli is with the Laboratoire d'Océanographie Physique et Biogéochimique, UMR-CNRS-IRD 6535, Centre d'Océanologie de Marseille, Université de la Méditerranée, 13288 Marseille Cedex, France (e-mail: francesco.nencioli@univmed.fr).

Y. Liu is with the State Key Laboratory of Oceanography in the Tropics, South China Sea Institute of Oceanology, Chinese Academy of Sciences, GuangZhou 510301, China, and also with the Graduate University of the Chinese Academy of Sciences, Beijing 100039, China (e-mail: liuy255@scsio.ac.cn).

Color versions of one or more of the figures in this paper are available online at <http://ieeexplore.ieee.org>.

Digital Object Identifier 10.1109/LGRS.2011.2155029

the enormous amount of remotely sensed SST measurements, eddy analysis based on manual detection is practically impossible, and therefore, automated eddy detection approaches are required. Some automated eddy detection approaches were developed in the literature: An edge detection scheme [1] was used to automatically detect eddies shed from the Gulf Stream [2]; a neural-network-based approach was developed to identify eddies from SST images [3]; another method involved the combination of edge detection and flow fields between two consecutive SST images [4]; and isothermal lines of the SST field were also proposed for automatic eddy detection [5].

This letter introduces an automated approach to detect eddies from SST data following a velocity–geometry eddy detection scheme for numerical modeled results developed by authors. The SST field is first converted to a vector field (thermal-wind velocity). The characteristics of the vector field are then used to detect and track eddies. The algorithm is written in MATLAB language. Since it is based on eddy geometry, it is simple and straightforward compared with the aforementioned SST eddy detection schemes.

II. METHODOLOGY

To better demonstrate the automated eddy detection algorithm, we use realistic remotely sensed SST data from the Remote Sensing System (REMSS) SST product as a test. The REMSS SST is a merged product from the SST data measured by both infrared sensors (Moderate Resolution Imaging Spectroradiometer (MODIS), high resolution but sensitive to cloud coverage) and microwave sensors (Advanced Microwave Scanning Radiometer for Earth Observing System (AMSR-E) and Tropical Rainfall Measuring Mission (TRMM) Microwave Images (TMI), not impacted by clouds but with coarse resolution) with all gaps filled using optimum interpolation [6]. Its spatial resolution is 9 km, and temporal sampling frequency is daily, which can well resolve mesoscale eddies. For more information about the product, please refer to its Web site www.remss.com. It should be noted that the REMSS SST product, as other SST products, carries some errors from either instruments or algorithms [7] that could confuse the eddy detection; we do not try to quantify this problem here.

Eddy analysis from the SST field is performed through the following steps: First, the thermal-wind velocity field is derived from the SST fields; then, an automated detection method is applied to the velocity field to identify eddy centers; for each detected center, eddy boundaries are computed from the

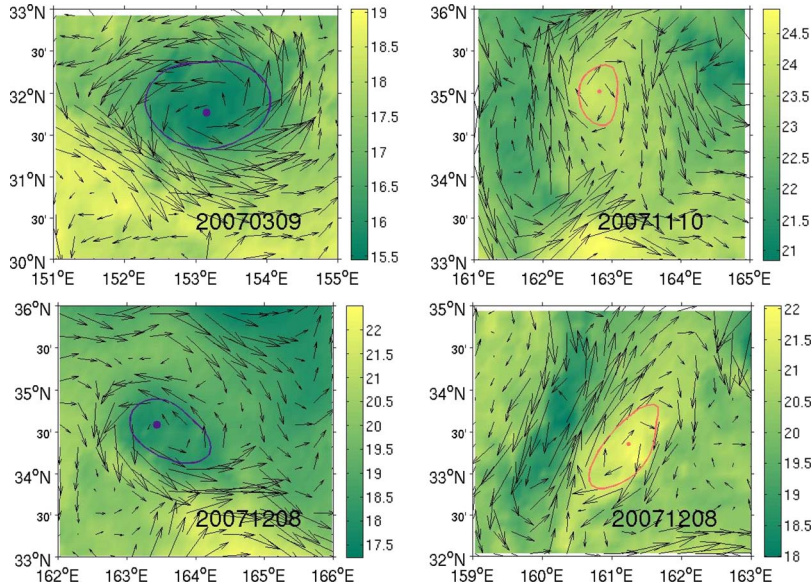


Fig. 1. Examples of (left panel) cyclonic and (right panel) anticyclonic eddies. Vectors are thermal-wind velocities, and color is SST. The solid lines are eddy boundaries.

closed contours of the SST fields; and finally, eddy tracks are reconstructed by comparing eddy fields detected at successive time steps.

The next paragraphs provide a detailed description of each of the aforementioned steps.

Step 1: Thermal-Wind Velocity

A Gaussian smoothing is applied to the original SST field to reduce the noise in the realistic SST data. A Sobel gradient operator [8] is then applied to the smoothed SST data to calculate SST gradients. This operator uses two 3×3 kernels which are convolved with the SST data to calculate approximations of their spatial derivatives. One kernel is used for the meridional direction, and the other is used for the zonal direction. Then, two matrices, containing the two approximations of the meridional and zonal derivatives for each point, G_x and G_y , respectively, are computed as follows:

$$\begin{aligned}
 \mathbf{G}_y &= \begin{bmatrix} +1 & +2 & +1 \\ 0 & 0 & 0 \\ -1 & -2 & -1 \end{bmatrix} * \mathbf{A} \\
 \mathbf{G}_x &= \begin{bmatrix} +1 & 0 & -1 \\ +2 & 0 & -2 \\ +1 & 0 & -1 \end{bmatrix} * \mathbf{A}
 \end{aligned} \tag{1}$$

where $*$ here denotes the 2-D convolution operation and \mathbf{A} is a matrix containing the SST data divided by the grid spacing at each point.

We can then define a vector $V = (U_x, U_y)$ as

$$\begin{aligned}
 U_x &= -G_y; U_y = G_x \text{ in the northern hemisphere} \\
 U_x &= G_y; U_y = G_x \text{ in the southern hemisphere.}
 \end{aligned} \tag{2}$$

In the two hemispheres, the sense of rotation of cyclonic (anticyclonic) eddies is opposite: counterclockwise (clockwise) in the northern hemisphere and clockwise (counterclockwise)

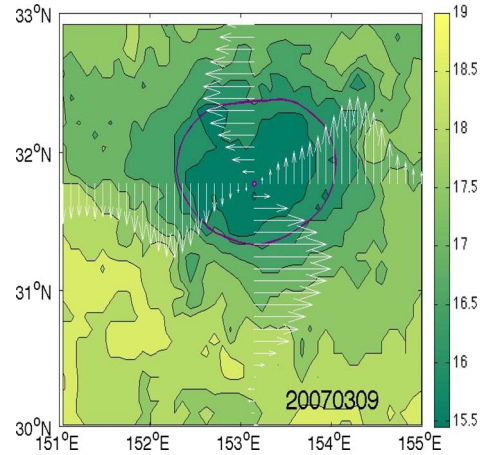


Fig. 2. Thermal-wind velocity profile across a cyclonic eddy.

in the southern hemisphere; however, the SST anomalies at the eddy centers remain colder (warmer) for cyclonic (anticyclonic) eddies. The vector $V (U_x, U_y)$ defined earlier guarantees V to have the correct sense of rotation around a cyclonic (anticyclonic) eddy on both hemispheres. The magnitude of the vector is simply the magnitude of the SST gradient. Fig. 1 shows examples of the vectors derived for two cold-core and two warm-core eddies in the Kuroshio Extension (KE) region. The vectors rotate anticlockwise (clockwise) around cold-core (warm-core) eddies, as it occurs as the velocity field associated with cyclonic and anticyclonic eddies. Based on the thermal-wind relationship and the first-order (linear) water state equation, it can be easily verified that the vector corresponds to the component of the baroclinic velocity contributed by temperature, thus the thermal-wind velocity (another component is a haline wind velocity contributed by the salinity). The component is the dominant one when the temperature field is the major contributor to the density variation. It should be noted that the vector defined in (2) represents only one component of

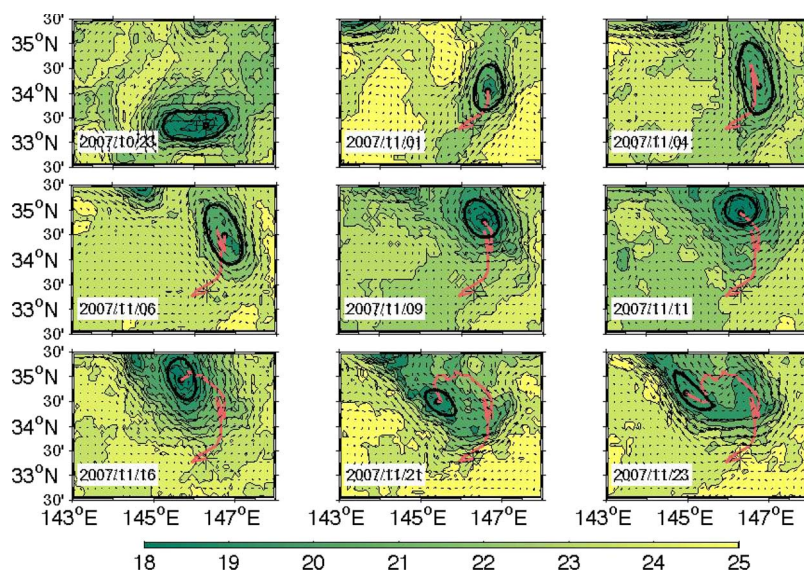


Fig. 3. Example of eddy tracking: The eddy is tracked over one month. The color is denoted to be SST, black circles are eddy boundaries, and the red lines are the path of eddy centers.

the absolute surface water flow (after multiplied by a coefficient $F = H * g / (f \rho_0)$, where H is the thermal-wind depth, g is the gravity constant, f is the Coriolis coefficient, and ρ_0 is the reference density). However, in the practice of eddy detection scheme, it is not necessary to convert the vector to the velocity unit with the aforementioned constant coefficient F .

Step 2: Detect Eddy Centers From Thermal-Wind Velocity Field

The method adopted in the algorithm was originally developed for automatic eddy detection from high-resolution numerical simulations [9], [10]. It is based on some of the features that characterize the velocity field associated with mesoscale eddies, e.g., [11], such as minimum velocities in the proximity of the eddy center and tangential velocities that increase approximately linearly with distance from the center before reaching a maximum value and then decaying. Since the thermal-wind velocity field computed in Step 1 has features similar to the real velocity field, as shown in Fig. 2, the method can be applied to detect eddy centers from V .

Four constraints are defined based on the characteristics of eddy velocity fields.

- 1) Along an east–west section, U_y has to reverse in sign across the eddy center, and its magnitude has to increase away from it.
- 2) Along a north–south section, U_x has to reverse in sign across the eddy center, and its magnitude has to increase away from it. The sense of rotation has to be the same as for it.
- 3) The thermal-wind velocity magnitude has a local minimum at the eddy center.
- 4) Around the eddy center, the directions of the thermal-wind velocity vectors have to change with a constant sense of rotation, and the directions of two neighboring thermal-wind velocity vectors have to lay within the same or two adjacent quadrants (the four quadrants are defined

by the north–south and west–east axes: the first quadrant encompasses all the directions from east to north; the second quadrant, the directions from north to west; the third quadrant, the directions from west to south; and the fourth quadrant, the directions from south to east).

These constraints are applied to each point of the thermal-wind velocity field. The points for which all four are satisfied are detected as eddy centers. In Figs. 1 and 2, black and red dots indicate detected centers of cyclonic and anticyclonic eddies, respectively.

Step 3: Calculate an Eddy's Size

After an eddy center is detected, the algorithm computes the eddy boundaries. Assuming that the eddy interior is the region where SST gradient magnitude decreases radially from the center, eddy limits can be defined as the outermost closed isothermal line around the eddy's center, across which the magnitude of the SST gradient starts to increase in the radial direction. The variation of the SST gradient magnitude across the closed contour is checked only at its four extremes (i.e., its northernmost, easternmost, southernmost, and westernmost points), which represents a reasonable tradeoff between computational efficiency and algorithm accuracy. It would be computationally too expensive to compute the variation across each point of the closed contour; by choosing the four extremes, the variation is checked at the most distant points from the eddy center along each of the main directions, regardless of the ellipticity and orientation of the eddy. Therefore, the selected points are where a decrease in the SST gradient magnitude is most likely to occur. Boundaries of cyclonic and anticyclonic eddies are marked with black and red solid lines, respectively, in Figs. 1 and 2.

Step 4: Track an Eddy Evolution

After eddy centers are detected for the entire SST data set, eddy tracks are determined by comparing the centers at

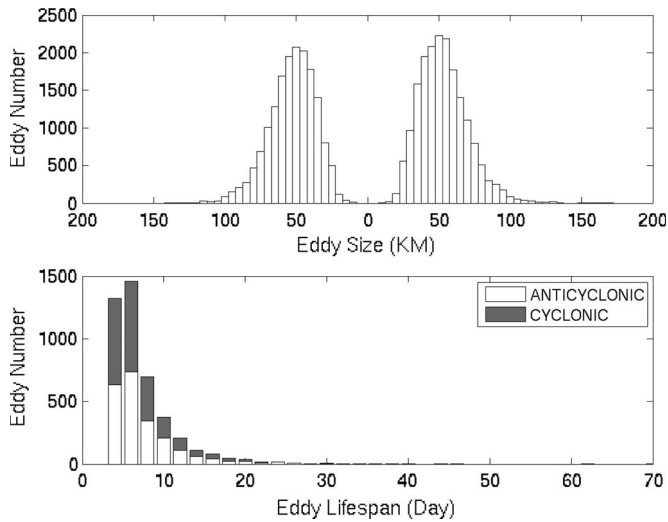


Fig. 4. Histograms of (upper) eddy sizes and (lower) eddy lifetimes. On the upper panel, the left and right sides of “0” on the x -axis denote the anticyclonic and cyclonic eddies, respectively. On the upper panel, an eddy on each step during its life time is considered as a separate eddy because it might have different size. On the lower panel, eddies on each step of its lifetime are considered as one item.

successive time steps. An eddy center at time step t is connected to an eddy center at time step $t + 1$ if the center at $t + 1$ is of the same type and within a searching area of $N \times N$ grid points around the center at t . If no centers are found at $t + 1$, a second search at $t + 2$ on a larger area $(N + N/2) \times (N + N/2)$ is performed. If, even at $t + 2$, no centers are found, then the eddy is considered dissipated, and the track closed. The size of the searching area needs to be accurately tuned: In order to avoid track splitting (i.e., divide a continuous track into multiple tracks), eddies cannot travel outside the searching area from one time step to the successive step. For this reason, the size of the searching area has to be defined depending on the spatial and temporal resolution of the data set, as well as on the characteristics of the mean flow field. Since eddies’ moving speed is about in a scale of 10 cm/s [12], for daily data, we choose 15 km as the search radius. Fig. 3 shows an example of tracking a cold core.

III. APPLICATION AND SUMMARY

As an example, the present algorithm is applied to the 2006–2008 REMSS SST data set at 9-km spatial resolution from the KE region $[140^\circ \text{ E} - 179^\circ \text{ E}] \times [28^\circ \text{ N} - 41^\circ \text{ N}]$. After its separation from the east coast of Japan, the Kuroshio becomes an eastward jet, which is particularly unstable without the constraint from the coast. The KE has long been recognized as a region rich in energetic pinched-off eddies [13].

Fig. 4 shows the histogram of the computed eddy sizes in the region, evident in a symmetric size distribution for cyclonic and anticyclonic eddies. Only the eddies that last at least five days are included in the analysis in order to remove SST anomalies which do not represent cohesive eddies. The most frequent eddy size is about 50 km, which is close to the first baroclinic deformation radius. The computed eddy sizes are slightly smaller than eddies (60–70 km) detected from satellite-

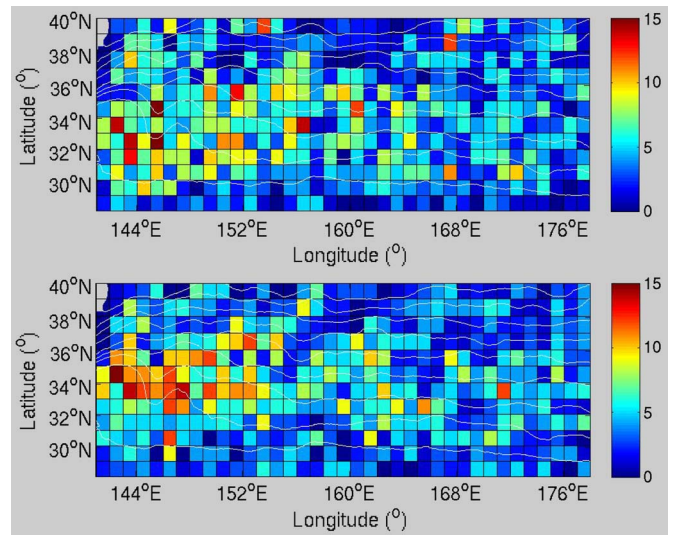


Fig. 5. Distribution of number of eddies generation number in a bin $1^\circ \times 1^\circ$ (eddy lifetime is longer than five days) in the KE region: (Upper) Cyclonic eddies and (lower) anticyclonic eddies. The white solid lines are isothermal lines from 15° C to 23° C with an interval of 1° C , calculated from the mean SST field averaged over 2006–2008.

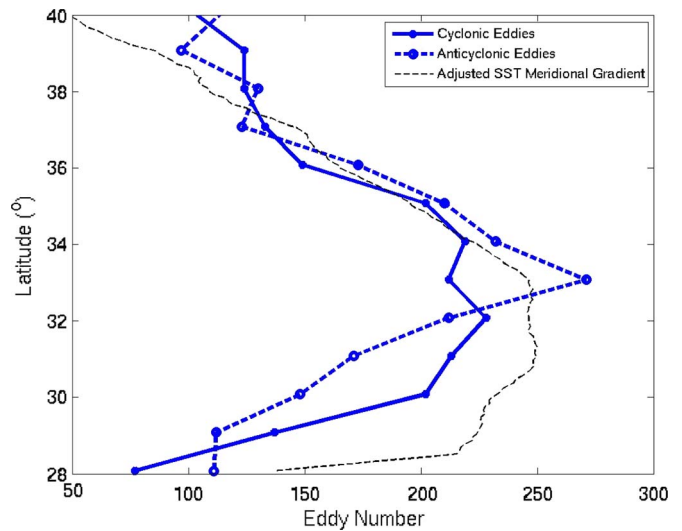


Fig. 6. Numbers of eddy generated per latitude: (Solid line) Cyclonic and (thick dashed line) anticyclonic. Only eddies with a lifetime longer than five days are included. The thin dashed line is the meridional gradient of SST (scaled to fit with the x -axis range). The meridional gradient of SST is negative; therefore, the peak represents the minimum gradient magnitude.

altimetry-measured sea surface level height anomaly (SSHA) data [14], and their average lifetimes are conspicuously shorter. This could be caused by the fact that the two data sets have different spatial resolutions and that they measure different properties (SST and SSHA). The latter raises an interesting question about how well an SSHA-defined eddy overlaps with its SST-defined counterpart. However, this is beyond the scope of this letter and will be discussed in future work. The eddy lifetimes also span symmetrically between cyclonic and anticyclonic eddies. The spatial distribution of eddy generation number, shown in Fig. 5, shows that most eddies occur along the Kuroshio path, shown in the contours of the SST field. Analysis

of the total eddy distribution with latitude shows that cyclonic (anticyclonic) eddies are more frequent on the south (north) of the Kuroshio path (see Fig. 6), as also observed from the analysis of eddies detected from the SSHA data [14].

This letter introduces a simple, effective, and automated oceanic eddy detection scheme for remotely sensed SST data. A thermal-wind velocity is derived from the SST data, which can be used to characterize the eddy structure represented by the SST. Based on the geometric feature of the thermal-wind velocity field associated with an eddy, an automated eddy detection scheme is developed to detect eddies from the SST data. The method includes the identification of eddy centers and the computation of eddy size, polarity, intensity, and lifetime tracking. The algorithm is applied to a high eddy activity zone, i.e., the KE region.

ACKNOWLEDGMENT

Microwave OI SST data are produced by Remote Sensing Systems and sponsored by National Oceanographic Partnership Program (NOPP), the NASA Earth Science Physical Oceanography Program, and the NASA MEaSUREs DISCOVER Project. Data are available at <http://www.remss.com>.

REFERENCES

- [1] J. Canny, "A computational approach to edge detection," *IEEE Trans. Pattern Anal. Mach. Intell.*, vol. PAMI-8, no. 6, pp. 679–698, Nov. 1986.
- [2] R. Holyer and S. Peckinpaugh, "Edge detection applied to satellite imagery of the oceans," *IEEE Trans. Geosci. Remote Sens.*, vol. 27, no. 1, pp. 46–56, Jan. 1989.
- [3] M. Castellani, "Identification of eddies from sea surface temperature maps with neural networks," *Int. J. Remote Sens.*, vol. 27, no. 8, pp. 1601–1618, Apr. 2006.
- [4] A. Fernandes and S. Nascimento, "Automatic water eddy detection in SST maps using random ellipse fitting and vectorial fields for image segmentation," in *Discovery Science*, vol. 4265. Berlin, Germany: Springer-Verlag, 2006, pp. 77–88.
- [5] D. D'Alimonte, "Detection of mesoscale eddy-related structures through iso-SST patterns," *IEEE Geosci. Remote Sens. Lett.*, vol. 6, no. 2, pp. 189–193, Apr. 2009.
- [6] C. L. Gentemann, P. J. Minnett, J. M. Sienkeiwicz, M. DeMaria, J. Cummings, Y. Jin, J. D. Doyle, L. Gramer, C. N. Barron, K. S. Casey, and C. J. Donlon, "The multi-sensor improved sea surface temperature (MISST) project," *Oceanography*, vol. 22, no. 2, pp. 76–87, 2009.
- [7] R. Reynolds and D. Chelton, "Comparisons of daily sea surface temperature analyses for 2007–08," *J. Clim.*, vol. 23, no. 13, pp. 3545–3562, Jul. 2010. DOI: 10.1175/2010JCLI3294.1.
- [8] I. Sobel and G. Feldman, "A 3×3 isotropic gradient operator for image processing," presented at the Stanford Artificial Project, Stanford, CA, 1968.
- [9] F. Nencioli, C. Dong, T. Dickey, L. Washburn, and J. McWilliams, "A vector geometry based eddy detection algorithm and its application to high-resolution numerical model products and high-frequency radar surface velocities in the Southern California Bight," *J. Atmos. Ocean. Technol.*, vol. 27, no. 3, pp. 564–579, Mar. 2010. DOI: 10.1175/2009JTECHO725.1.
- [10] C. Dong, T. Mavor, F. Nencioli, S. Jiang, Y. Uchiyama, J. C. McWilliams, T. Dickey, M. Ondrusek, H. Zhang, and D. K. Clark, "An oceanic cyclonic eddy on the lee side of Lanai Island, Hawaii," *J. Geophys. Res.*, vol. 114, p. C10008, 2009. DOI: 10.1029/2009JC005346.
- [11] T. D. Dickey, F. Nencioli, V. S. Kuwahara, C. Leonard, W. Black, Y. M. Rii, R. R. Bidigare, and Q. Zhang, "Physical and bio-optical observations of oceanic cyclones west of the island of Hawaii," *Deep Sea Res. II*, vol. 55, no. 10–13, pp. 1195–1217, May/June 2008.
- [12] D. B. Chelton, M. G. Schlax, and R. M. Samelson, "Global observations of nonlinear mesoscale eddies," *Prog. Oceanogr.*, 2010, in press. DOI: 10.1016/j.pocean.2011.01.002.
- [13] B. Qiu and S. Chen, "Eddy-mean flow interaction in the decadal-modulating Kuroshio Extension system," *Deep-Sea Res.*, vol. 57, no. 13/14, pp. 1098–1110, Jul. 2010. DOI: 10.1016/j.dsr2.2008.11.036.
- [14] S. Itoh and I. Yasuda, "Characteristics of mesoscale eddies in the Kuroshio-Oyashio extension region detected from the distribution of the sea surface height anomaly," *J. Phys. Oceanogr.*, vol. 40, no. 5, pp. 1018–1034, May 2010. DOI: 10.1175/2009JPO4265.1.